Evaluation of multiaxial stress-strain models and fatigue life prediction methods under proportional loading

Marco Antonio Meggiolaro, Jaime Tupiassú Pinho de Castro

Department of Mechanical Engineering, Pontifical Catholic University of Rio de Janeiro, Rio de Janeiro/RJ – Brazil

Antonio Carlos de Oliveira Miranda

Tecgraf, Pontifical Catholic University of Rio de Janeiro, Rio de Janeiro/RJ – Brazil

Abstract

Multiaxial fatigue damage occurs when the principal stress directions vary during the loading induced by several independent forces, such as out-of-phase bending and torsion. Uniaxial damage models cannot be reliably applied in this case. Besides the need for multiaxial damage models, another key issue to reliably model such problems is how to calculate the elastic-plastic stresses from the multiaxial strains. Hooke's law cannot be used to correlate stresses and strains for short lives due to plasticity effects. Ramberg-Osgood cannot be used either to directly correlate principal stresses and strains under multiaxial loading, because this model has been developed for the uniaxial case. The purpose of this work is to critically review and compare the main fatigue crack initiation models under multiaxial loading. The studied models include stress-based ones such as Sines, Findley and Dang Van, and strain-based ones such as the γN curve, Brown-Miller, Fatemi-Socie and Smith-Watson-Topper models. Modified formulations of the strain-based models are presented to incorporate Findley's idea of using critical planes that maximize damage. To incorporate plasticity effects, four models are studied and compared to correlate stresses and strains under proportional loading: the method of the highest K_t, the constant ratio model, Hoffmann-Seeger's and Dowling's models.

Keywords: multiaxial fatigue, crack initiation, life prediction models, stress-strain models.

1 Introduction

Real loads can induce combined bending, torsional, axial and shear stresses, which can generate bi- or tri-axial variable stress/strain histories at the critical point (in general a notch root), causing the so-called multiaxial fatigue problems. The load history is said to be proportional when it generates stresses with principal axes which maintain a fixed orientation, while non-proportional loading is associated with principal directions which change in time during the loading history.

Mechanics of Solids in Brazil 2009, H.S. da Costa Mattos & Marcílio Alves (Editors)
Brazilian Society of Mechanical Sciences and Engineering, ISBN 978-85-85769-43-7

For periodic loads with same frequency, one can also define the concept of in-phase and out-of-phase loading. In-phase loading always leads to proportional histories, however the opposite is not true: e.g., the stresses $\sigma_x = \sigma_I$ and $\sigma_y = \sigma_{II}$ induced on a plate by perpendicular ($\perp$) forces F_x and F_y are always proportional, because the principal axes maintain a fixed direction even if F_x and F_y are out-of-phase.

On the other hand, out-of-phase axial and torsional stresses always generate non-proportional (NP) loading [1]. The non-proportionality factor F_{np} of the applied loads can be obtained from the shape of the ellipsis that encloses the history of normal and shear strains induced by them, ε and γ. Considering a and b ($b \leq a$) as the semi-axes of the ellipsis which encloses the strain path in the Mises diagram $\varepsilon \times \gamma/\sqrt{3}$, then the non-proportionality factor F_{np} is defined as b/a ($0 \leq F_{np} \leq 1$), see Fig. 1. A further discussion on enclosing ellipses, and hyper-ellipsoids, can be found in [2].

All proportional loadings have shear strains γ proportional to the normal strains ε, with $F_{np} = 0$ and a straight-line trajectory in the $\varepsilon \times \gamma/\sqrt{3}$ diagram. Any loading history with $F_{np} > 0$ is NP. Note e.g. that the loading ($\sigma_a \sin \omega t + \tau_a \cos \omega t$) with $\tau_a = \sigma_a \sqrt{3/2}(1 + \nu)$, caused by a traction and a properly scaled torsion 90° out of phase, has $F_{np} = 1$, therefore the maximum possible non-proportionality.

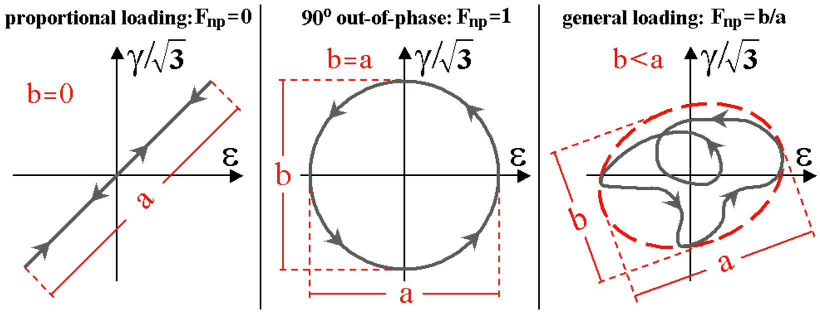

Figure 1: Diagram $\varepsilon \times \gamma/\sqrt{3}$, and associated non-proportionality factors (Socie and Marquis, 1999).

Predictions with NP histories can be very complex, because they involve at least three potential problems:

1. NP hardening: the cyclic hardening coefficient H_c and the ratio $\Delta\sigma/\Delta\varepsilon$ of a few materials increase under NP loading, which significantly decreases the fatigue life of parts subject to a constant $\Delta\varepsilon$;
2. Damage calculation: the SN and εN curves, measured under proportional loading, cannot be directly used when principal directions vary, because in this case the crack propagation plane in general does not match the one from the tests; and
3. Cycle counting: the traditional rain-flow counting techniques cannot be applied to variable amplitude NP loading, because the peaks and valleys of ε in general do not match with the ones of γ, becoming impossible to decide *a priori* which points should be accounted for.

The first two problems will be addressed in this work. A NP hardening model will be presented, to allow for the correct calculation of the equivalent stresses, and multiaxial models based on stress or strain measurements will be used to calculate the damage generated both by proportional and NP loadings.

A few classical models that correlate stresses or strains with multiaxial fatigue life are studied below. Stress-based models (which can be applied for long life predictions) proposed by Sines, Findley and Dang Van are presented, as well as strain-based models proposed by Brown-Miller, Fatemi-Socie and Smith-Watson-Topper (SWT), which must be used for short lives.

One problem with the application of the Fatemi-Socie or SWT models is the need to calculate the elastic-plastic stresses from the multiaxial strains, because Ramberg-Osgood is only valid for uniaxial stresses. Another challenge in multiaxial fatigue life calculations is the modeling of the notch effect. The elastic stress concentration factor K_σ and strain concentration factor K_ε are the same for uniaxial loading, but in general in the multiaxial case K_σ is different from K_ε even under elastic stresses.

Therefore, even in the elastic case, it is not trivial to study the notch effect under multiaxial loading. The problem is worse in the elastic-plastic case, where even uniaxial loadings can generate NP multiaxial stress and strain histories, due to the tri-axial stress state at the notch root and to the difference between the elastic and plastic Poisson coefficients. Typically, metallic alloys have $1/4 \leq \nu_{el} \leq 1/3$ and $\nu_{pl} = 0.5$. In the following sections the multiaxial stress-strain models are presented and compared, including notch effects.

2 Non-proportional loading

A few materials under NP cyclic loading can harden much more than it would be predicted from the traditional cyclic $\sigma\varepsilon$ curve. This phenomenon, called NP hardening, depends on the load history (through the NP factor F_{np}) and on the material (through a constant α_{np} of NP hardening, where $0 \leq \alpha_{np} \leq 1$). The NP hardening can be modeled in general using the same Ramberg-Osgood plastic exponent h_c from the uniaxial cyclic σ-ε curve, and using a new coefficient $H_{cnp} = H_c \cdot (1 + \alpha_{np} \cdot F_{np})$, where H_c is the uniaxial Ramberg-Osgood plastic coefficient, see Fig. 2. Note that the NP hardening can multiply the uniaxial strain hardening coefficient H_c by a value as high as 2.

The largest NP hardening occurs when $F_{np} = 1$, e.g. under a properly scaled traction-torsion loading 90^o out of phase which generates a circle in the $\varepsilon \times \gamma/\sqrt{3}$ Mises diagram.

Typically, the NP hardening effect is high in austenitic stainless steels at room temperature ($\alpha_{np} \cong 1$ in the stainless steel 316), medium in carbon steels ($\alpha_{np} \cong 0.3$ in the 1045 steel) and low in aluminum alloys ($\alpha_{np} \cong 0$ for Al 7075). Note that proportional histories do not lead to NP hardening.

The NP hardening happens in materials with low fault stacking energy (which in austenitic stainless steels is only 23mJ/m^2) and well spaced dislocations, where the slip bands generated by proportional loading are always planar. In these materials, the NP loads activate crossed slip bands in several directions (due to the rotation of the maximum shear planes), therefore increasing the hardening effect ($\alpha_{np} \gg 0$) with respect to the proportional loadings. But in materials with high fault stacking energy (such as aluminum alloys, with a typical value of 250mJ/m^2) and with close dislocations, the crossed slip bands already happen naturally even under proportional loading, therefore the NP histories do not cause any significant difference in hardening ($\alpha_{np} \cong 0$).

But the Coffin-Manson or the Morrow crack initiation equations cannot account for the influence of

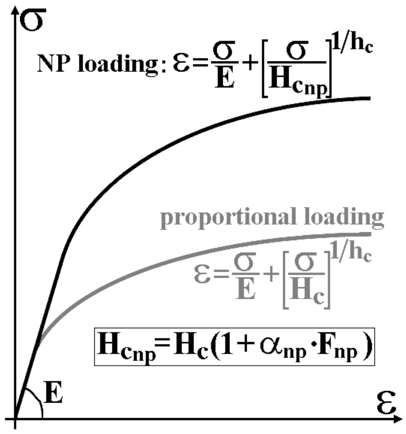

Figure 2: Effect of cyclic NP loadings on the NP hardening.

NP hardening. This implies that the use of traditional εN equations, which were developed to model uniaxial fatigue problems, can be non-conservative when the loading histories are NP.

However, it must be noted that the NP hardening reduces fatigue life only in strain-controlled problems (such as in εN specimen tests or very sharp notches, e.g.), because the stresses $\Delta\sigma$ caused by a given $\Delta\varepsilon$ are higher than in the proportional case. But in stress-controlled problems (the most common case in practice), the $\Delta\varepsilon$ generated by a given $\Delta\sigma$ is lower under NP loading, therefore the fatigue life is higher than in the proportional case (the uniaxial εN equations can lead to conservative predictions in this case). In the following sections, the multiaxial models to predict NP damage are studied.

3 Stress-based multiaxial fatigue damage models

It is well known that Tresca or Mises equivalent stresses must be used to predict crack initiation lives, which depend on the cyclic movement of dislocations. However, crack initiation can and should be divided into:

- formation of microcracks, which is almost insensitive to mean stresses and hydrostatic pressure in metals, because it only depends on dislocation movement; followed by
- propagation of the dominant microcrack, which also depends on the crack face opening and the friction between the faces, becoming increasingly sensitive to the applied mean stress σ_m as the microcrack grows.

Microcracks are cracks with sizes up to the order of the metal grain sizes. Their modeling using classical fracture mechanics is questionable, as opposed to long cracks (typically larger than 1 or 2mm), which have crack propagation rates controlled by ΔK.

However, SN and εN tests bring test specimens (TS) to fracture, or to the generation of a small, finite crack, therefore they include both microcrack initiation and propagation phases. Thus, since the shear stress $\Delta\tau$ controls the initiation of a microcrack, while the normal stress $\sigma_\perp$ perpendicular to its plane (or the hydrostatic stress σ_h, invariant defined as the mean of the normal stresses) controls its opening, both are important to predict the fatigue lives of SN and εN specimens.

In fact, a component under uniaxial traction $\sigma_x = \sigma$ and another under torsion $\tau_{xy} = \sigma/2$ work under the same Tresca equivalent stress, but the microcracks on the plane of τ_{max} in the first component are subject to a normal stress $\sigma_\perp$ perpendicular to that plane that tends to keep their mouth open, exposing the crack tips and decreasing the crack face friction, see Fig. 3. Therefore, the fatigue damage generated by $\Delta\sigma$ can be greater than the one caused by the pure torsion $\Delta\tau = \Delta\sigma/2$.

The Mises equivalent stress is able to, at least in part, consider such effect, because the component under torsion would have $\sigma_{Mises} = \tau_{xy}\sqrt{3} = 0.866 \cdot \sigma_x < \sigma$, however σ_{Mises} is insensitive to the hydrostatic stress σ_h. The Mises shear strain τ_{Mises}, which acts on the octahedric planes, does not consider as well the effects of σ_h, relating with σ_{Mises} through:

$$\begin{aligned}\sigma_{Mises} &= \frac{3}{\sqrt{2}}\tau_{Mises} = \frac{1}{\sqrt{2}}\sqrt{(\sigma_1-\sigma_2)^2+(\sigma_1-\sigma_3)^2+(\sigma_2-\sigma_3)^2} = \\ &= \frac{1}{\sqrt{2}}\sqrt{(\sigma_x-\sigma_y)^2+(\sigma_y-\sigma_z)^2+(\sigma_x-\sigma_z)^2+6(\tau_{xy}^2+\tau_{yz}^2+\tau_{xz}^2)}\end{aligned} \tag{1}$$

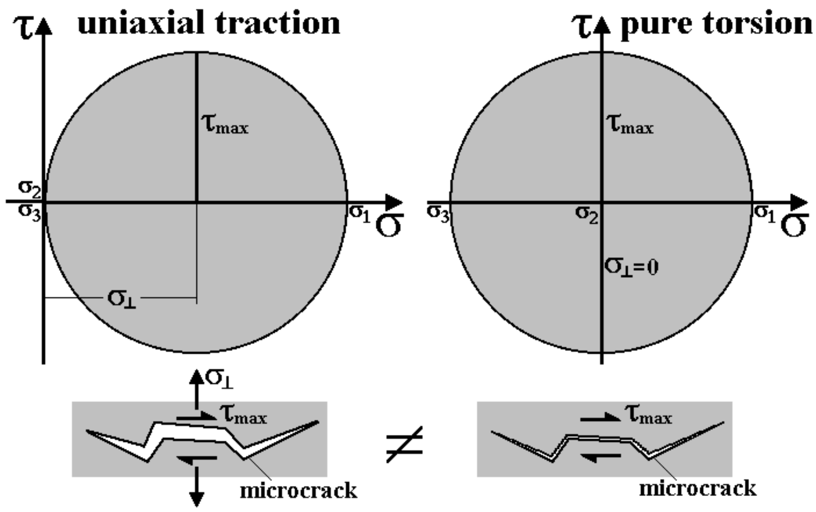

Figure 3: Mohr circles showing why under the same $\Delta\sigma_{Tresca}$ equivalent loading the component under pure torsion can have a higher fatigue life than the one under pure traction.

Sines [3] has proposed a fatigue failure criterion under proportional multiaxial stresses, based on $\Delta\tau_{Mises}$ and on $\sigma_{hm} = (\sigma_{xm} + \sigma_{ym} + \sigma_{zm})/3$, the hydrostatic component of the mean stresses (insensitive to the shear stresses):

$$\frac{\Delta\tau_{Mises}}{2} + \alpha_S \cdot (3 \cdot \sigma_{h_m}) = \beta_S \tag{2}$$

where α_S and β_S are adjustable constants for each material, and

$$\Delta\tau_{Mises} = \frac{1}{3}\sqrt{(\Delta\sigma_1 - \Delta\sigma_2)^2 + (\Delta\sigma_1 - \Delta\sigma_3)^2 + (\Delta\sigma_2 - \Delta\sigma_3)^2} \tag{3}$$

In this way, according to the Sines criterion, a component will have infinite fatigue life under proportional loading if

$$\Delta\tau_{Mises}/2 + \alpha_S \cdot (3 \cdot \sigma_{hm}) < \beta_S \tag{4}$$

On the other hand, the Findley [4] criterion, which is also applicable to NP multiaxial loadings, assumes that the crack initiates at the critical plane of the critical point. This idea is interesting, because it is on this plane that the damage caused by the combination $\Delta\tau/2 + \alpha_F \cdot \sigma_\perp$ is maximum, where $\Delta\tau/2$ is the shear stress amplitude on that plane and $\sigma_\perp$ is the normal stress perpendicular to it. Thus, according to Findley the fatigue failure criterion at the critical plane of the critical point is

$$\left(\frac{\Delta\tau}{2} + \alpha_F \cdot \sigma_\perp\right)_{\max} = \beta_F \tag{5}$$

where α_F and β_F are constants which must be fitted by measurements in at least two types of fatigue tests, e.g., under rotating bending and under pure torsion, or in push-pull tests under two different R ratios.

The critical plane can vary at each i-th event of the NP loads, even when the critical point remains the same, but Findley predicts fatigue failure based on the plane where the sum of the damages associated with $[\Delta\tau_i(\theta)/2 + \alpha_F \cdot \sigma_{\perp i}(\theta)]$ is maximum, where θ is the angle of such plane with respect to a reference direction.

Under pure torsion, Eq. (5) can be written as

$$\sqrt{1 + \alpha_F^2} \cdot \frac{\Delta\tau}{2} = \beta_F \tag{6}$$

And under cyclic uniaxial traction with alternate component σ_a and maximum component σ_{max}, it can be shown that Findley's criterion can be written as

$$0.5\sigma_a \left[\sqrt{1 + \left(\frac{2\alpha_F}{1-R}\right)^2} + \frac{2\alpha_F}{1-R}\right] = \beta_F \tag{7}$$

where $R = \sigma_{min}/\sigma_{max}$ is the stress ratio, which quantifies the mean stress effects.

Therefore, from Findley it is possible to estimate the fatigue limit $S_L(R)$ under any ratio R from α_F and the fatigue limit S_L (obtained under zero mean loads, i.e., with $R = -1$, see Fig. 4) through

$$\frac{S_L(R)}{S_L} = \frac{\sigma_a(R)}{\sigma_a} = \frac{\sqrt{1+\alpha_F^2}+\alpha_F}{\sqrt{1+\left(\frac{2\alpha_F}{1-R}\right)^2}+\frac{2\alpha_F}{1-R}} \tag{8}$$

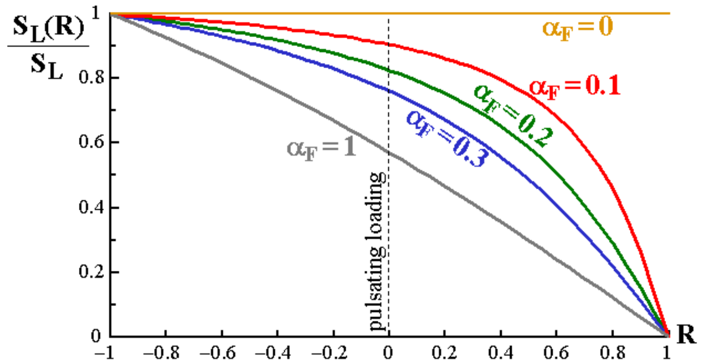

Figure 4: Fatigue limit $S_L(R)$ as a function of R, according to Findley.

From the principle that the damage associated with the initiation of fatigue microcracks cannot be detected from macroscopic measurements, Dang Van [5] proposed a model that considers the variable micro stresses that act inside a characteristic volume element (VE) of the material, where the macroscopic stresses and strains are supposedly constant. The VE is the unit used in structural analysis to represent the material properties, such as its Young modulus and its several strengths. Thus the VE must be small compared to the component's dimensions, but large compared to the parameter that characterizes the intrinsic anisotropy of the material. For instance, a VE of only 1mm^3 is sufficient for most structural metal alloys, which have a grain size g typically between 10 and 100μm (the grain itself, being a monocrystal, is intrinsically anisotropic).

Inside a VE, the local micro stresses $[\sigma_{ij}]_\mu = \sigma_\mu$ and strains $[\varepsilon_{ij}]_\mu = \varepsilon_\mu$ acting between grains, or between them and small imperfections such as inclusions, e.g., can significantly differ from the macro stresses $[\sigma_{ij}]_M = \sigma_M$ and strains $[\varepsilon_{ij}]_M = \varepsilon_M$, assumed constant in the macroscopic analysis normally used in mechanical design. Therefore, these micro quantities can significantly influence crack initiation. Note that if the term "microscopic" is reserved to the scale associated with interatomic stresses, domain of solid state physics, then its is recommended to use the term "mesoscopic" to describe the intra or intergranular stresses. Thus, the macroscopic stresses reflect the average of the mesoscopic stresses in a VE: $\sigma_M = \int \sigma_\mu dV/V$, where V is the volume of the VE. Similarly, $\varepsilon_M = \int \varepsilon_\mu dV/V$.

In other words, the macroscopic stresses and strains are assumed constant at the characteristic volume element VE of the material, however the mesoscopic intergranular stresses can vary a lot, influencing crack initiation.

Since the microcracks initiate at persistent slip bands, Dang Van assumed that fatigue damage was caused by the mesoscopic shear strain history τ_μ(t) and influenced by the mesoscopic hydrostatic stress history $\sigma_{\mu h}$(t). The simplest failure criterion involving these components is the linear combination given by:

$$\tau_\mu(t) + \alpha_{DV} \cdot \sigma_{\mu_h}(t) = \beta_{DV} \tag{9}$$

Note that the Sines, Findley and Dang Van criteria can be included in the general class of Mohr models against material failure, which use combinations of the shear stress τ that acts on a certain plane with the normal or hydrostatic stresses σ on this plane:

$$\tau + \alpha \cdot \sigma = \beta \tag{10}$$

The Sines criterion uses the Mises or octahedric plane and the hydrostatic stresses, therefore $\tau \equiv \Delta\tau_{Mises}/2$, $\sigma \equiv 3 \cdot \sigma_{hm}$, $\alpha \equiv \alpha_S$, $\beta \equiv \beta_S$; Findley uses the shear stress on the critical plane and the normal stress perpendicular to it, thus $\tau \equiv \Delta\tau/2$, $\sigma \equiv \sigma_\perp$, $\alpha \equiv \alpha_F$, $\beta \equiv \beta_F$; and Dang Van can be obtained from $\tau \equiv \tau_\mu(t)$, $\sigma \equiv \sigma_{\mu h}(t)$, $\alpha \equiv \alpha_{DV}$, $\beta \equiv \beta_{DV}$. Other similar criteria can be found in [1] and [6].

Finally, it is important to remember that the SN and εN tests involve both microcrack initiation (sensitive to τ) and propagation (more sensitive to σ) phases, and therefore fatigue damage can be more influenced by τ or σ, depending on the percentage of the life spent at each phase. Therefore, materials with large values of α are more sensitive to σ (normal stresses are more important to them), probably spending more cycles to propagate than to initiate the microcrack.

4 Strain-based multiaxial fatigue damage models

The three multiaxial failure criteria presented above are based on macroscopic stresses that are supposedly elastic, therefore they are only applicable when σ_{Mises} is much smaller than the cyclic yielding strength S_{yc}. Thus, as in the case of the SN method, they should only be used to predict long fatigue lives. Otherwise, it is imperative to use fatigue damage criteria based on applied strains instead of stresses [1], using the principles studied in the so-called εN method.

One of the simplest models is the one based on the γN curve, similar to Coffin-Manson's equation, which uses the largest shear strain range $\Delta\gamma_{max}$ acting on the specimen (γ_{ij} ($2\varepsilon_{ij}$, $i \neq j$) to predict fatigue life

$$\frac{\Delta\gamma_{\max}}{2} = \frac{\tau_c}{G}(2N)^{b_\gamma} + \gamma_c(2N)^{c_\gamma} \tag{11}$$

where τ_c, b_γ, γ_c and c_γ are parameters similar to the ones used in Coffin-Manson's equation. In this way, since the shear modulus $G = E/\left[2(1+\nu)\right]$, ν being Poisson's coefficient, if no experimental data is available, then the γN curve can be estimated assuming $\tau_c \cong \sigma_c/\sqrt{3}$, $b_\gamma \cong b$, $\gamma_c \cong \varepsilon_c\sqrt{3}$ and $c_\gamma \cong c$, resulting in

$$\frac{\Delta\gamma_{\max}}{2} \cong \frac{\sigma_c}{E}\frac{2(1+\nu)}{\sqrt{3}}(2N)^b + \varepsilon_c\sqrt{3}(2N)^c \tag{12}$$

The γN curve is only recommended to model fatigue damage in materials that are more sensitive to shear strains (which have small α in the Mohr models), and if the mean loads are zero. It would be expected that such materials would have a shorter torsional fatigue life than similar materials more sensitive to normal stresses.

The Brown-Miller [7] model can consider the mean stress effects, combining the maximum range of the shear strain $\Delta\gamma_{max}$ to the range of normal strain $\Delta\varepsilon_\perp$ (through the term $\Delta\gamma_{max}/2 + \alpha_{BM}\cdot\Delta\varepsilon_\perp$) and the mean normal stress $\sigma_{\perp m}$ perpendicular to the plane of maximum shear strain, to obtain the fatigue life N:

$$\frac{\Delta\gamma_{\max}}{2} + \alpha_{BM}\cdot\Delta\varepsilon_\perp = \beta_1\frac{\sigma_c - 2\sigma_{\perp m}}{E}(2N)^b + \beta_2\varepsilon_c(2N)^c \tag{13}$$

where α_{BM} is a fitting parameter ($\alpha_{BM} \cong 0.3$ for ductile metals in lives near the fatigue limit), $\beta_1 = (1+\nu+(1-\nu)\cdot\alpha_{BM}$, and $\beta_2 = 1.5 + 0.5\cdot\alpha_{BM}$.

This equation was adapted from Morrow to fit uniaxial traction test data, where the mean stress σ_m is equal to $2\sigma_{\perp m}$ (because $\sigma_{\perp m}$ acts perpendicularly to the plane of γ_{max}, therefore it is worth half of σ_m).

The values of β_1 and β_2 are obtained assuming uniaxial traction, see Fig. 5:

$$\left.\begin{array}{l}\Delta\gamma_{\max} = (1+\nu)\Delta\varepsilon \\ \Delta\varepsilon_\perp = (1-\nu)\Delta\varepsilon/2\end{array}\right\} \Rightarrow \frac{\Delta\gamma_{\max}}{2} + \alpha_{BM}\Delta\varepsilon_\perp = \frac{\Delta\varepsilon}{2}\left[(1+\nu) + \alpha_{BM}(1-\nu)\right] \tag{14}$$

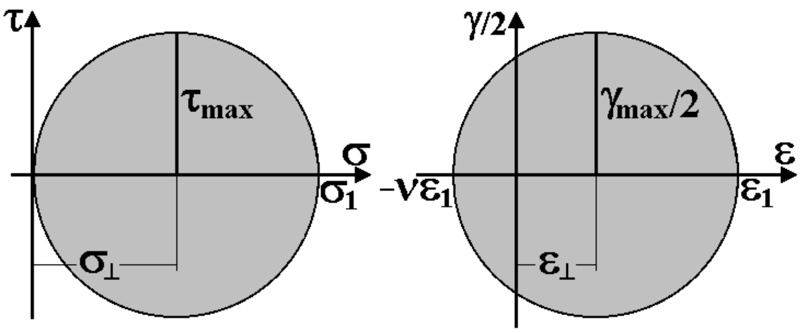

Figure 5: Mohr circles for stresses and strains under uniaxial traction.

From Eq. (14), the coefficients $\beta_1 = (1+\nu) + (1-\nu)\cdot\alpha_{BM}$ and $\beta_2 = 1.5 + 0.5\cdot\alpha_{BM}$ are obtained, because $\nu = 0.5$ for plastic strains, which preserve volume. The original Brown-Miller model assumes that the elastic strains have $\nu = 0.3$, therefore $\beta_1 \cong (1+0.3) + (1-0.3)\cdot\alpha_{BM} = 1.3 + 0.7\cdot\alpha_{BM}$.

The Brown-Miller model is frequently used in multiaxial fatigue, even though it is not reasonable to assume that $\Delta\varepsilon_\perp$ can control the opening and closure of microcracks, because the range $\Delta\varepsilon$ does not include information about maximum stresses or strains. E.g., two microcracks with the same $\Delta\gamma_{max}$ and $\Delta\varepsilon_\perp$ can have very different fatigue lives if one is opened (under traction) and the other closed (under compression) due to the mean load effect. The use of $\sigma_{\perp m}$ compensates in part for this model flaw, however the mean stress effect is only considered in the elastic part.

Fatemi and Socie [8] suggested replacing $\Delta\varepsilon_\perp$ by the maximum normal stress $\sigma_{\perp max}$ perpendicular to the plane of maximum shear strain, applying it to the γN curve:

$$\frac{\Delta\gamma_{\max}}{2}\left(1 + \alpha_{FS}\frac{\sigma_{\perp\max}}{S_{yc}}\right) = \frac{\tau_c}{G}(2N)^{b_\gamma} + \gamma_c(2N)^{c_\gamma} \tag{15}$$

Note that the value of α_{BM} and α_{FS} indicates whether the material is more sensitive to τ (α_{BM} or $\alpha_{FS} \ll 1$) or to σ (α_{BM} or $\alpha_{FS} \gg 1$).

If the propagation phase of the microcracks (more sensitive to σ) is dominant over initiation, the Smith-Watson-Topper (SWT) multiaxial model can be used [9]:

$$\frac{\Delta\varepsilon_1}{2}\cdot\sigma_{\perp 1\max} = \frac{\sigma_c^2}{E}(2N)^{2b} + \sigma_c\varepsilon_c(2N)^{b+c} \tag{16}$$

where $\Delta\varepsilon_1$ is the range of the maximum principal strain and $\sigma_{(1max}$ is the stress peak in the direction perpendicular to ε_1.

Figure 6 summarizes the parameters used in the above strain-based models. In addition, there are several other models based on the plastic energy dissipated by the hysteresis loops, and other combining energy with critical planes, see [1].

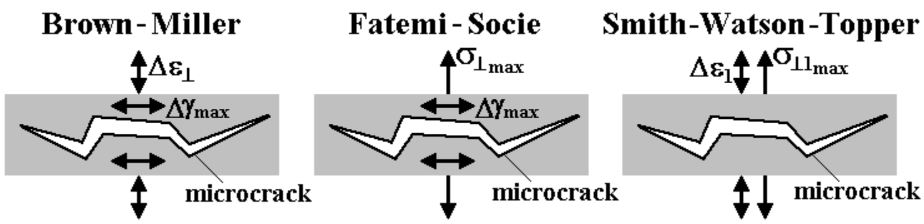

Figure 6: Parameters which affect the strain-based multiaxial models.

It is important to note that the plane of maximum shear strain amplitude $\Delta\gamma_{max}/2$ (used in Brown-Miller's and Fatemi-Socie's models) is in general different from the planes that would maximize the respective damage parameters ($\Delta\gamma/2 + \alpha_{BM}(\Delta\varepsilon_\perp$ for Brown-Miller, and $\Delta\gamma((1 + \alpha_{FS}(\sigma_{\perp max}/S_{yc})/2$

for Fatemi-Socie). But if these are the parameters that cause damage, it is reasonable to argue that fatigue life should be calculated on the critical plane that maximizes them (in a similar way as done in Findley's model), and not on the plane of $\Delta\gamma_{max}$. In this way, it is a good idea to modify the Brown-Miller and Fatemi-Socie models introducing a subtle but important change:

$$\frac{\Delta\gamma_{\max}}{2} + \alpha_{BM} \cdot \Delta\varepsilon_{\perp} \Rightarrow \left(\frac{\Delta\gamma}{2} + \alpha_{BM} \cdot \Delta\varepsilon_{\perp}\right)_{\max} \tag{17}$$

$$\frac{\Delta\gamma_{\max}}{2}\left(1 + \alpha_{FS}\frac{\sigma_{\perp\max}}{S_{yc}}\right) \Rightarrow \left(\frac{\Delta\gamma}{2} + \alpha_{FS}\frac{\Delta\gamma}{2}\frac{\sigma_{\perp\gamma}}{S_{yc}}\right)_{\max} \tag{18}$$

The use of critical planes that maximize the damage parameters in each model has the advantage of predicting not only the fatigue life but also the dominant planes where the crack will initiate. However, these calculations are not simple and require the use of sophisticated numerical methods.

This idea can also be applied to the SWT model, calculating the critical plane where the product between the normal strain range $\Delta\varepsilon_{\perp}$ and the normal stress peak $\sigma_{\perp max}$ is maximized, adopting the modification

$$\frac{\Delta\varepsilon_1}{2} \cdot \sigma_{\perp 1\max} \Rightarrow \left(\frac{\Delta\varepsilon_{\perp}}{2} \cdot \sigma_{\perp\max}\right)_{\max} \tag{19}$$

A great advantage of the Fatemi-Socie (or SWT) model is to be able to consider the effect of NP hardening from the peak of normal stress $\sigma_{\perp max}$ (or $\sigma_{\perp 1max}$). In stainless steels, e.g., a NP history leads to a much higher damage than a proportional one with the same $\Delta\gamma_{max}$ and $\Delta\varepsilon_{\perp}$, because the NP hardening increases the value of $\sigma_{\perp max}$ (or $\sigma_{\perp 1max}$). Note that Brown-Miller would wrongfully predict the same damage in both histories (because $\Delta\gamma_{max}$ and $\Delta\varepsilon_{\perp}$ would be the same), and only the Fatemi-Socie and SWT models would be able to correctly account for the greater damage of the NP loading (assuming that H_{cnp} would be used to obtain $\sigma_{\perp max}$ and $\sigma_{\perp 1max}$).

5 Multiaxial stress-strain relations

Hooke's law cannot be used to correlate stresses and strains for short multiaxial fatigue life predictions, due to plasticity effects. The hookean stresses and strains, $\tilde{\sigma}$ and $\tilde{\varepsilon}$, defined as the values of σ and ε obtained assuming that the material would be linear elastic (using Hooke's law and, at the notches, considering elastic K_σ and K_ε), can only be applied for long life predictions.

In addition, Ramberg-Osgood cannot be used either to directly correlate principal stresses and strains σ_i and ε_i (i = 1, 2, 3) of a multiaxial history, because this model has been developed for the uniaxial case.

However, if the elastic nominal stress range $\Delta\sigma_n$ is caused by in-phase loading, then it is trivial to calculate the elastic-plastic stresses and strains at the notch root using the "highest K_t method". In this approximate method, the equivalent nominal stress range $\Delta\sigma_n$ calculated from Tresca or Mises is used to obtain $\Delta\sigma$ and $\Delta\varepsilon$ at the notch root using Ramberg-Osgood and (for safety, because the method is conservative) the highest K_t in Neuber's rule. Remember that the multiaxial loadings can result, at the same notch root, in different values of K_t for traction, bending, torsion and shear loadings, but only the maximum one is used. To generate more accurate predictions for notches under combined stresses, it is recommended to use multiaxial σ-ε relations.

Several models have been proposed to correlate σ_i and ε_i in proportional histories, e.g.: the constant ratio model [1], Hoffmann-Seeger's model ([10], and Dowling's model [11]. To present these three models, it is necessary to define a few variables involved in their formulation:

- $\tilde{\sigma}_1$, $\tilde{\sigma}_2$, $\tilde{\sigma}_3$, $\tilde{\varepsilon}_1$, $\tilde{\varepsilon}_2$, $\tilde{\varepsilon}_3$: hookean principal stresses and strains at the notch root (elastically calculated using Hooke's law and elastic K_σ and K_ε);
- $\tilde{\sigma}_{Mises}$, $\tilde{\varepsilon}_{Mises}$: hookean Mises stress and strain (at the notch root), calculated using the above variables;
- σ_1, σ_2, σ_3, ε_1, ε_2, ε_3: elastic-plastic principal stresses and strains (notch root);
- σ_{Mises}, ε_{Mises}: Mises stress and strain (notch root);
- λ_2, λ_3: ratios between pairs of principal stresses, where $\lambda_2 = \sigma_2/\sigma_1$ and $\lambda_3 = \sigma_3/\sigma_1$, both between -1 and 1;
- φ_2, φ_3: ratios between pairs of principal strains, where $\varphi_2 = \varepsilon_2/\varepsilon_1$, $\varphi_3 = \varepsilon_3/\varepsilon_1$, both between -1 and 1; and
- λ_{Mises}, φ_{Mises}: Mises ratios $\lambda_{Mises} = \sigma_{Mises}/\sigma_1$ and $\varphi_{Mises} = \varepsilon_{Mises}/\varepsilon_1$.

From the above definitions, it is possible to obtain

$$\lambda_{Mises} = \frac{\sigma_{Mises}}{\sigma_1} = \frac{1}{\sqrt{2}}\sqrt{(1-\lambda_2)^2 + (1-\lambda_3)^2 + (\lambda_2-\lambda_3)^2} \tag{20}$$

$$\phi_{Mises} = \frac{\varepsilon_{Mises}}{\varepsilon_1} = \frac{1}{\sqrt{2}(1+\nu)}\sqrt{(1-\phi_2)^2 + (1-\phi_3)^2 + (\phi_2-\phi_3)^2} \tag{21}$$

The three models are described next.

5.1 Constant ratio model

The *constant ratio model* [1] assumes that, under a proportional history, the bi-axial ratios λ_2, λ_3, φ_2 and φ_3 remain constant even after yielding has occurred. Since the elastic Poisson coefficient ν_{el} is typically between 1/4 and 1/3 in most metal alloys, significantly different than the plastic $\nu_{pl} = 0.5$, these ratios are in fact not constant, but for small plastic strains this is a good approximation.

Thus, these ratios can be estimated from the elastic (hookean) stresses and strains, obtained from Hooke's law using elastic K_σ and K_ε:

$$\lambda_2 \cong \frac{\tilde{\sigma}_2}{\tilde{\sigma}_1},\ \lambda_3 \cong \frac{\tilde{\sigma}_3}{\tilde{\sigma}_1},\ \phi_2 \cong \frac{\tilde{\varepsilon}_2}{\tilde{\varepsilon}_1},\ \phi_3 \cong \frac{\tilde{\varepsilon}_3}{\tilde{\varepsilon}_1} \tag{22}$$

Therefore, λ_{Mises} is also a constant, leading to

$$\lambda_{Mises} \cong \frac{\tilde{\sigma}_{Mises}}{\tilde{\sigma}_1} \Rightarrow \tilde{\sigma}_{Mises} \cong \frac{\tilde{\sigma}_1}{\sqrt{2}}\sqrt{(1-\lambda_2)^2 + (1-\lambda_3)^2 + (\lambda_2-\lambda_3)^2} \tag{23}$$

and, similarly, φ_{Mises} can be calculated from φ_2 and φ_3. The cyclic σ-ε relation is then defined using Mises and the Ramberg-Osgood uniaxial parameters

$$\varepsilon_{Mises} = \frac{\sigma_{Mises}}{E} + \left(\frac{\sigma_{Mises}}{H_c}\right)^{1/h_c} \tag{24}$$

If no notches are present, then the above equation is used together with the estimates for λ_{Mises}, φ_{Mises}, λ_2, λ_3, φ_2 and φ_3 to obtain σ_i from ε_i (i = 1, 2, 3), or vice-versa. In notched components, $\tilde{\sigma}_{Mises}$ (elastically calculated including the K_ts) is applied to a variation of the Neuber's rule to calculate the Mises elastic-plastic stress σ_{Mises} and, finally, ε_{Mises}, σ_i and ε_i (i = 1, 2, 3):

$$\frac{(\tilde{\sigma}_{Mises})^2}{E} = \sigma_{Mises} \cdot \varepsilon_{Mises} = \frac{(\sigma_{Mises})^2}{E} + \sigma_{Mises} \cdot \left(\frac{\sigma_{Mises}}{H_c}\right)^{1/h_c} \tag{25}$$

After calculating σ_{Mises} and ε_{Mises}, the constant ratio model obtains the principal stress and strain using:

$$\begin{cases} \sigma_1 = \sigma_{Mises}/\lambda_{Mises},\ \sigma_2 = \lambda_2\sigma_1,\ \sigma_3 = \lambda_3\sigma_1 \\ \varepsilon_1 = \varepsilon_{Mises}/\phi_{Mises},\ \varepsilon_2 = \phi_2\varepsilon_1,\ \varepsilon_3 = \phi_3\varepsilon_1 \end{cases} \tag{26}$$

5.2 Hoffmann-Seeger's model

Hoffmann-Seeger's model [10] uses the same cyclic σ-ε relation and the same variation of Neuber's rule presented above to calculate σ_{Mises} and ε_{Mises}, but it assumes that:

- the critical point happens at the surface, with principal stresses σ_1 and σ_2;
- σ_3 is defined normal to the surface, therefore $\sigma_3 = 0$ (and then $\lambda_3 = 0$); and
- only the ratio $\phi_2 = \tilde{\varepsilon}_2/\tilde{\varepsilon}_1$ is estimated using the linear elastic (hookean) values.

After calculating σ_{Mises} and ε_{Mises}, σ_i and ε_i are estimated from:

$$\begin{cases} \sigma_1 = \sigma_{Mises}/\bar{\lambda}_{Mises},\ \sigma_2 = \bar{\lambda}_2\sigma_1,\ \sigma_3 = 0 \\ \varepsilon_1 = \frac{(1-\bar{\lambda}_2\bar{\nu})\varepsilon_{Mises}}{\bar{\lambda}_{Mises}},\ \varepsilon_2 = \phi_2\varepsilon_1,\ \varepsilon_3 = -\bar{\nu}\varepsilon_1\frac{1+\bar{\lambda}_2}{1-\bar{\lambda}_2\bar{\nu}} \end{cases} \tag{27}$$

$$\bar{\nu} = \frac{1}{2} - \frac{(1/2 - \nu_{el})\sigma_{Mises}}{E \cdot \varepsilon_{Mises}},\ \bar{\lambda}_2 = \frac{\phi_2 + \bar{\nu}}{1 + \phi_2\bar{\nu}},\ \bar{\lambda}_{Mises} = \sqrt{1 - \bar{\lambda}_2 + \bar{\lambda}_2^2} \tag{28}$$

5.3 Dowling's model

The model proposed in [11] also assumes that the principal stresses σ_1 and σ_2 act on the surface of the critical point (therefore σ_3 is zero), and it considers λ_2 and φ_2 constant, estimating them from their hookean values

$$\lambda_2 = \frac{\sigma_2}{\sigma_1} \cong \frac{\tilde{\sigma}_2}{\tilde{\sigma}_1} \cong \frac{\phi_2 + \nu}{1 + \phi_2\nu},\ \phi_2 = \frac{\varepsilon_2}{\varepsilon_1} \cong \frac{\tilde{\varepsilon}_2}{\tilde{\varepsilon}_1} \cong \frac{\lambda_2 - \nu}{1 - \lambda_2\nu} \tag{29}$$

Exceptionally, σ_2 is defined here as the lowest principal stress at the surface, even if σ_2 is smaller than σ_3 (i.e. the convention $\sigma_3 \leq \sigma_2 \leq \sigma_1$ is violated if $\lambda_2 < 0$).

The greatest difference between the previous two models and Dowling's is that the latter correlates σ_1 and ε_1 directly using effective Ramberg-Osgood parameters E^* and H_c^*

$$E^* = \left(\frac{1+\phi_2\nu}{1-\nu^2}\right)\cdot E,\ H_c^* = H_c\cdot\left(\frac{2}{2-\lambda_2}\right)^{h_c}(1-\lambda_2+\lambda_2{}^2)^{0.5(h_c-1)} \tag{30}$$

and the effective relation between σ_1 and ε_1 is [11]

$$\varepsilon_1 = \frac{\sigma_1}{E^*} + \left(\frac{\sigma_1}{H_c{}^*}\right)^{1/h_c} \tag{31}$$

Figure 7 presents the principal stress-strain relation for the 1020 steel, according to Dowling's model.

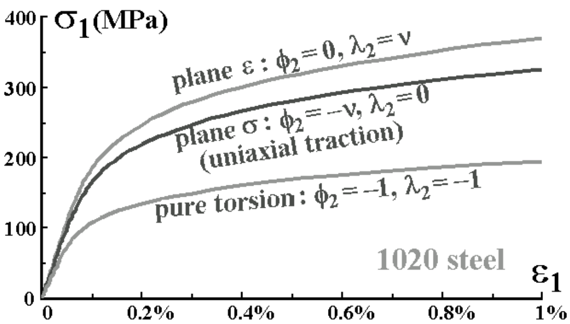

Figure 7: Principal stress-strain relations under plane strain, plane stress and pure torsion, according to Dowling.

In notched components, another variation of Neuber's rule must be used to calculate σ_1 (and then ε_1) from $\tilde{\sigma}_{Mises}$:

$$\frac{(\tilde{\sigma}_{Mises})^2}{E} = \sigma_1\cdot\varepsilon_1 = \frac{\sigma_1^2}{E^*} + \sigma_1\cdot\left(\frac{\sigma_1}{H_c^*}\right)^{1/h_c} \tag{32}$$

The other principal stresses and strains are obtained from σ_1 and ε_1:

$$\begin{gathered}\sigma_2 = \lambda_2\sigma_1,\ \sigma_3 = 0\\ \varepsilon_2 = \phi_2\varepsilon_1,\ \varepsilon_3 = -\bar{\nu}\varepsilon_1\tfrac{1+\lambda_2}{1-\lambda_2\bar{\nu}},\ \bar{\nu} = \tfrac{1}{2} - \left(\tfrac{1}{2}-\nu\right)\tfrac{\sigma_1}{E^*\varepsilon_1}\end{gathered} \tag{33}$$

The largest shear strain γ_{max} can then be calculated from the maximum difference between the principal strains ε_i (i = 1, 2, 3), obtaining not only its magnitude but also the plane where this maximum occurs.

It is important to note that the three presented models (formulated using the cyclic σ-ε curve) can also be applied to the hysteresis loops equations, by replacing in each equation ε with $\Delta\varepsilon/2$ and also σ with $\Delta\sigma/2$. The presented models are compared next.

6 Comparison among the multiaxial models

The presented multiaxial models are compared considering a notched 1020 steel shaft with diameter d equal to 60mm under alternate bending moment M_a of 2kNm and torsion T_a of 3kNm, in phase, with stress concentration factors in bending K_{tM} equal to 3.4 and in torsion K_{tT} equal to 2.4.

Assuming the alternate nominal stress σ_{na} as elastic,

$$\sigma_{n_a} = \frac{\sqrt{(32M_a)^2 + 3(16T_a)^2}}{\pi d^3} \tag{34}$$

then $\sigma_{na} = 155$MPa. This stress is lower than the cyclic yielding strength S$_{yc}$= 241MPa, therefore the hypothesis of σ_{na} elastic is valid.

Using the "highest K_t method" through the highest $K_t = 3.4$, σ_a and ε_a are calculated using Mises and Neuber

$$(K_t\sigma_{n_a})^2 = (3.4 \cdot 155)^2 = \sigma_a\varepsilon_a E = \sigma_a{}^2 + 203000 \cdot \sigma_a\left(\frac{\sigma_a}{772}\right)^{1/0.18} \Rightarrow \begin{cases} \sigma_a = 279MPa \\ \varepsilon_a = 0.49\% \end{cases} \tag{35}$$

and then the life N estimated for the shaft is

$$\frac{\Delta\varepsilon}{2} = \varepsilon_a = \frac{896}{203000}(2N)^{-0.12} + 0.41(2N)^{-0.51} \Rightarrow N = 5871\ cycles \tag{36}$$

To use the multiaxial stress-strain models, the hookean stresses at the notch root are calculated considering $K_{tM} = 3.4$ and $K_{tT} = 2.4$ as purely elastic:

$$\tilde{\sigma}_{a_{Mises}} = \sqrt{(K_{tM}\sigma_M)^2 + 3(K_{tT}\tau_T)^2} = \frac{\sqrt{(3.4 \cdot 32 \cdot M_a)^2 + 3(2.4 \cdot 16 \cdot T_a)^2}}{\pi(0.060)^3} \tag{37}$$

$$\tilde{\sigma}_{a_{1,2}} = \frac{K_{tM}\sigma_M}{2} \pm \sqrt{\left(\frac{K_{tM}\sigma_M}{2}\right)^2 + (K_{tT}\tau_T)^2} = 160 \pm 234MPa \tag{38}$$

Thus, the hookean stresses are $\tilde{\sigma}_{a_{Mises}} = 435$MPa, $\tilde{\sigma}_{a_1} = 394$MPa, $\tilde{\sigma}_{a_2} =$ -73MPa and $\tilde{\sigma}_{a_3} = 0$, which can be correlated to the principal hookean strains from Hooke's law (considering $\nu = 0.3$):

$$\begin{aligned} \tilde{\varepsilon}_{a_1} &= [394 - 0.3(-73 + 0)]/203000 = 0.205\% \\ \tilde{\varepsilon}_{a_2} &= [-73 - 0.3(394 + 0)]/203000 = -0.094\% \\ \tilde{\varepsilon}_{a_3} &= [0 - 0.3(-73 + 394)]/203000 = -0.047\% \end{aligned} \tag{39}$$

$$\tilde{\varepsilon}_{a_{Mises}} = \frac{1}{\sqrt{2}(1+\nu)}\sqrt{(\tilde{\varepsilon}_{a_1} - \tilde{\varepsilon}_{a_2})^2 + (\tilde{\varepsilon}_{a_1} - \tilde{\varepsilon}_{a_3})^2 + (\tilde{\varepsilon}_{a_2} - \tilde{\varepsilon}_{a_3})^2} = 0.214\% \tag{40}$$

From the constant ratio and Hoffmann-Seeger models,

$$\frac{\tilde{\sigma}^2_{a_{Mises}}}{E} == 0.93 = \frac{{\sigma_{aMises}}^2}{E} + \sigma_{a_{Mises}} \cdot \left(\frac{\sigma_{a_{Mises}}}{772}\right)^{1/0.18} \Rightarrow \sigma_{a_{Mises}} = 259MPa \tag{41}$$

$$\varepsilon_{a_{Mises}} = \frac{\sigma_{aMises}}{203000} + \left(\frac{\sigma_{aMises}}{772}\right)^{1/0.18} \Rightarrow \varepsilon_{a_{Mises}} = 0.360\% \tag{42}$$

Note, as expected, that $\sigma_{a_{Mises}} < \tilde{\sigma}_{a_{Mises}}$ and $\varepsilon_{a_{Mises}} > \tilde{\varepsilon}_{a_{Mises}}$.

From the constant ratio model, the hookean stresses and strains can be used to estimate $\lambda_{Mises} =$ 1.105, $\lambda_2 =$ -0.185, $\lambda_3 = 0$, $\varphi_{Mises} =$ 1.046, $\varphi_2 =$ -0.460 and $\varphi_3 =$ -0.231, so the alternate principal stresses and strains are

$$\begin{aligned} &\sigma_{a_1} = 259/1.1 = 235MPa,\ \sigma_{a2} = \lambda_2\sigma_{a_1} = -44MPa,\ \sigma_{a3} = 0 \\ &\varepsilon_{a_1} = 0.359\%/1.046 = 0.344\%,\ \varepsilon_{a_2} = \phi_2\varepsilon_{a1} = -0.158\%,\ \varepsilon_{a_3} = \phi_3\varepsilon_{a_1} = -0.080\% \end{aligned} \tag{43}$$

On the other hand, Hoffmann-Seeger's model predicts

$$\begin{aligned} &\bar{\nu} = \frac{1}{2} - \left(\frac{1}{2} - \nu\right)\frac{\sigma_{a_{Mises}}}{E \cdot \varepsilon_{a_{Mises}}} = 0.5 - 0.2\frac{259}{203000 \cdot 0.00359} = 0.429 \\ &\bar{\lambda}_2 = \frac{\phi_2 + \bar{\nu}}{1 + \phi_2\bar{\nu}} = \frac{-0.46 + \bar{\nu}}{1 - 0.46\bar{\nu}} = -0.0387,\ \bar{\lambda}_{Mises} = \sqrt{1 - \bar{\lambda}_2 + \bar{\lambda}_2^2} = 1.02 \end{aligned} \tag{44}$$

resulting in alternate principal stresses and strains

$$\begin{cases} \sigma_{a_1} = 259/1.02 = 254MPa,\ \sigma_{a_2} = -0.0387 \cdot \sigma_{a_1} = -10MPa,\ \sigma_{a_3} = 0 \\ \varepsilon_{a_1} = (1 - \bar{\lambda}_2\bar{\nu})0.360\%/1.02 = 0.359\%,\ \varepsilon_{a_2} = \phi_2\varepsilon_{a1} = -0.165\% \\ \varepsilon_{a_3} = -\bar{\nu}\varepsilon_{a_1}(1 + \bar{\lambda}_2)/(1 - \bar{\lambda}_2\bar{\nu}) = -0.146\% \end{cases} \tag{45}$$

Dowling's model uses the elastic ratios $\lambda_2 =$ -0.185 and $\varphi_2 =$ -0.460 to calculate the effective parameters of the hardening curve

$$E^* = \left(\frac{1 + \phi_2\nu}{1 - \nu^2}\right) \cdot E = \left(\frac{1 - 0.46 \cdot 0.3}{1 - 0.3^2}\right) \cdot 203GPa = 192GPa \tag{46}$$

$$H_c^* = 772MPa \cdot \left(\frac{2}{2 - \lambda_2}\right)^{0.18}(1 - \lambda_2 + {\lambda_2}^2)^{0.5(0.18-1)} = 700MPa \tag{47}$$

$$\frac{(\tilde{\sigma}_{a_{Mises}})^2}{E} = 0.93 = \sigma_{a1} \cdot \varepsilon_{a_1} = \frac{\sigma^2_{a_1}}{E^*} + \sigma_{a1} \cdot (\frac{\sigma_{a_1}}{H_c^*})^{1/h_c} \Rightarrow \begin{cases} \sigma_{a_1} = 240MPa \\ \varepsilon_{a_1} = 0.388\% \end{cases} \tag{48}$$

$$\begin{cases} \sigma_{a_2} = \lambda_2\sigma_{a_1} = -45MPa,\ \sigma_{a_3} = 0 \\ \varepsilon_{a_2} = \phi_2\varepsilon_{a_1} = -0.179\%,\ \varepsilon_{a3} = -\bar{\nu}\varepsilon_{a1}\frac{1+\lambda_2}{1-\lambda_2\bar{\nu}} = -0.127\%\ (\bar{\nu} = 0.436) \end{cases} \tag{49}$$

For all considered models, the maximum shear strain amplitude is calculated from $\gamma_{amax} = \varepsilon_{a1} - \varepsilon_{a2}$, assuming that the directions 1 and 2 are respectively the ones with maximum and minimum principal strains. The maximum normal strains and stresses in the plane of γ_{amax} are

$$\varepsilon_{a\perp} = (\varepsilon_{a1} + \varepsilon_{a_2})/2 \text{ and } \sigma_{a\perp} = (\sigma_{a_1} + \sigma_{a_2})/2 \tag{50}$$

Since in this problem the mean stresses and strains are zero, the values used by the Brown-Miller, Fatemi-Socie and SWT strain-life models are respectively $\Delta\varepsilon_\perp = 2\varepsilon_{a\perp}$, $\sigma_{\perp max} = \sigma_{a\perp}$ and $\sigma_{\perp 1max} = \sigma_{a_1}$.

Table 1 summarizes the stresses and strains obtained from the hookean values (obtained assuming elastic stresses, which must not be used in life predictions in the presence of significant plasticity), from the "highest K_t method", and from the three presented multiaxial stress-strain models: the constant ratio, Hoffmann-Seeger's and Dowling's.

Table 1: Stresses (in MPa) and strains predicted from the studied models.

	hookean values	highest K_t method	constant ratio	Hoffman-Seeger	Dowling
$\sigma_{a_{Mises}}$	435	279	259	259	265
$\varepsilon_{a_{Mises}}$	0.214%	0.488%	0.360%	0.360%	0.418%
σ_{a_1}	394	253	235	254	240
σ_{a_2}	-73	-47	-44	-10	-45
σ_{a_3}	0	0	0	0	0
ε_{a_1}	0.205%	0.466%	0.344%	0.359%	0.388%
ε_{a_2}	-0.094%	-0.215%	-0.158%	-0.165%	-0.179%
ε_{a_3}	-0.047%	-0.108%	-0.080%	-0.146%	-0.127%
$\gamma_{a_{max}}$	0.299%	0.681%	0.502%	0.524%	0.567%
$\Delta\varepsilon_\perp$	0.111%	0.251%	0.186%	0.194%	0.209%
$\sigma_{\perp max}$	160	103	95	122	98

Note from Table 1 that the "highest K_t method" is conservative, especially for the calculated strains, but not too much, therefore it could be used in practice. The three multiaxial models are in theory more accurate, predicting approximately the same values.

Now, using e.g. Dowling's model, the fatigue life N can be obtained from the several damage models. Considering the εN curve and using the Mises strain $\varepsilon_{a_{Mises}} = 0.418\%$, then it is found that $N = 8765$ cycles.

If, instead of the εN curve, the γN curve is considered, estimating its coefficients from $\tau_c \cong \sigma_c/\sqrt{3}$, $b_\gamma \cong b$, $\gamma_c \cong \varepsilon_c\sqrt{3}$ and $c_\gamma \cong c$, and using $\gamma_{a_{max}} = 0.567\%$, then it is found that $N = 14693$ cycles.

Considering the Brown-Miller's model, with its constants estimated from $\alpha_{BM} \cong 0.3$, $\beta_1 = 1.3 + 0.7 \cdot \alpha_{BM} = 1.51$ and $\beta_2 = 1.5 + 0.5 \cdot \alpha_{BM} = 1.65$, with $\Delta\varepsilon_\perp = 0.209\%$, then it is found that $N = 10290$ cycles.

Fatemi-Socie's model, using $\alpha_{FS} \cong S_{yc}/\sigma_c = 241\text{MPa}/896\text{MPa} \cong 0.27$ and the γN curve estimated as above, where $\sigma_{\perp max} = 98$MPa, results in $N = 11201$ cycles.

And finally, considering the SWT's model, which is appropriate for materials more sensitive to normal stresses, with $\Delta\varepsilon_1/2 = \varepsilon_{a_1} = 0.388\%$ and, since the mean loads are zero, $\sigma_{\perp 1max} = \sigma_{a_1} = 240$MPa, then $N = 13577$ cycles.

The above results, based on stresses and strains from Dowling's model, are recalculated considering hookean values, the "highest K_t method", the constant ratio and Hoffmann-Seeger models, using the ViDa fatigue design software [12, 13]. The results are shown in Table 2.

Table 2: Fatigue lives (in cycles) predicted from the studied multiaxial models.

	Mises + εN curve	γN curve	Brown-Miller	Fatemi-Socie	SWT
hookean values	59500	94300	63000	56200	18300
highest K_t method	5900	9120	6440	6940	8470
constant ratio	13000	20300	14100	15500	18300
Hoffmann-Seeger	13000	18100	12600	12900	14200
Dowling	8770	14700	10300	11200	13600

Except from the results obtained from the hookean values (which are significantly non-conservative), all combinations of multiaxial damage models with multiaxial stress-strain relations resulted in predicted lives not too different, varying between 5900 and 20300 cycles. Therefore, it is reasonable to consider in proportional histories the use of simplifications such as the "highest K_t method" and the εN curve applied to $\Delta\varepsilon_{Mises}/2$, despite the conservative predictions.

The hookean values result in poor estimates, overestimating σ_{a_1} and underestimating ε_{a_1}, but it interestingly estimates quite well the product $\sigma_{a_1}\varepsilon_{a1}$ (because, according to Neuber, $\tilde{\sigma}_{a_1}\tilde{\varepsilon}_{a_1} \cong \sigma_{a_1}\varepsilon_{a_1}$), therefore they resulted in good predictions when combined with SWT's model, which is based on this product.

But in NP histories, the NP hardening can have a significant effect in the fatigue life. In addition, none of the presented σ-ε models is valid in the NP case (because all of them assumed φ_2 constant). In the NP case, incremental plasticity models must be used [1].

7 Conclusions

In this work, the multiaxial damage models of Sines, Findley and Dang Van, applicable to long fatigue lives, and Brown-Miller, Fatemi-Socie and Smith-Watson-Topper (SWT), which consider plasticity, were reviewed. The Sines model is easy to compute, it considers the effect of the second principal stress σ_2 (because it uses the Mises plane), but it is only valid for proportional histories. On the other hand, Findley's model is hard to compute, because it requires the search for a critical plane, but for long lives it is valid for any load history, proportional or NP. Dang Van's model is able to consider the damage in a mesoscopic scale, but it has the limitations of the stress-based models.

The strain-based models are valid for any life, short or long. Among them, the Brown-Miller and Fatemi-Socie models give more value to the shear strains γ, while SWT does it for normal strains ε. Brown-Miller and Fatemi-Socie combine $\Delta\gamma_{max}$ to $\Delta\varepsilon_{\perp}$ or to $\sigma_{\perp max}$ normal to the direction of γ_{max}, being applicable to proportional or NP histories. SWT uses the principal strain ε_1. The most versatile models among the studied ones are the Fatemi-Socie and SWT, because they can include the NP hardening effect. But in order to generate a more realistic model, it is important to modify these criteria to calculate the fatigue life in the critical plane where the damage parameters of each model are maximized.

The main multiaxial stress-strain models were also reviewed and compared. It can be concluded that multiaxial stress-strain relations must be used instead of uniaxial ones, even though a few simplifications are adequate, such as the "highest K_t method" for notched components. Since the critical point of a structure is usually in its surface, in general a 2D analysis (under plane stress) is enough for multiaxial fatigue design. Except for the results from the hookean values, which are significantly non-conservative, all combinations of strain-based multiaxial damage models with multiaxial stress-strain relations resulted in not too different lives (within a factor of 2) for the considered example, which has significant plastic strains (but they were not much higher than the elastic ones). The best predictions should be the ones from multiaxial models that use the critical plane idea, where the damage parameters are maximized. However, none of the studied stress-strain models is valid for NP hardening, which can have a significant influence in the fatigue lives of e.g. stainless steels.

References

[1] Socie, D.F. & Marquis, G.B., Multiaxial fatigue. *SAE International*, 1999.

[2] Zouain, N., Mamiya, E.N. & Comes, F., Using enclosing ellipsoids in multiaxial fatigue strength criteria. *European Journal of Mechanics - A, Solids*, **25**, pp. 51–71, 2006.

[3] Sines, G., Behavior of metals under complex static and alternating stresses. *Metal Fatigue*, McGraw-Hill, pp. 145–169, 1959.

[4] Findley, W.N., A theory for the effect of mean stress on fatigue of metals under combined torsion and axial load or bending. *Journal of Engineering for Industry*, pp. 301–306, 1959.

[5] Dang Van, K. & Papadopoulos, I.V., *High-Cycle Metal Fatigue*. Springer, 1999.

[6] Gonçalves, C.A., Araújo, J.A. & Mamiya, E.N., Multiaxial fatigue: a stress based criterion for hard metals. *International Journal of Fatigue*, **27**, pp. 177–187, 2005.

[7] Brown, M. & Miller, K.J., A theory for fatigue under multiaxial stress-strain conditions. *Institute of Mech Engineers*, **187**, pp. 745–756, 1973.

[8] Fatemi, A. & Socie, D.F., A critical plane approach to multiaxial damage including out-of-phase loading. *Fatigue and Fracture of Eng Materials and Structures*, **11(3)**, pp. 149–166, 1988.

[9] Smith, R.N., Watson, P. & Topper, T.H., A stress-strain parameter for the fatigue of metals. *J of Materials*, **5(4)**, pp. 767–778, 1970.

[10] Hoffmann, M. & Seeger, T., A generalized method for estimating multiaxial elastic-plastic notch stresses

and strains, Part 1: Theory. *J Eng Materials & Technology*, **107**, pp. 250–254, 1985.

[11] Dowling, N.E., Brose, W.R. & Wilson, W.K., Notched member fatigue life predictions by the local strain approach. *Fatigue Under Complex Loading: Analysis and Experiments, AE-6, SAE*, 1977.

[12] Meggiolaro, M.A. & Castro, J.T.P., Vida 98 - danômetro visual para automatizar o projeto à fadiga sob carregamentos complexos. *Journal of the Brazilian Society of Mechanical Sciences*, **20(4)**, pp. 666–685, 1998.

[13] Miranda, A.C.O., Meggiolaro, M.A., Castro, J.T.P., Martha, L.F. & Bittencourt, T.N., Fatigue life and crack path prediction in generic 2D structural components. *Engineering Fracture Mechanics*, **70**, pp. 1259–1279, 2003.

Mechanics of Solids in Brazil 2009, H.S. da Costa Mattos & Marcílio Alves (Editors)
Brazilian Society of Mechanical Sciences and Engineering, ISBN 978-85-85769-43-7